

Heat conductivity of DNA double helix

Alexander V. Savin,¹ Mikhail A. Mazo,¹ Irina P. Kikot,¹ Leonid I. Manevitch,¹ and Alexey V. Onufriev²

¹*Semenov Institute of Chemical Physics, Russian Academy of Sciences, Moscow 119991, Russia*

²*Departments of Computer Science and Physics, 2160C Torgersen Hall, Virginia Tech, Blacksburg, VA 24061, USA*

A coarse-grain (CG) model of DNA double helix is proposed in which each base is represented by 6 grains; the grains interact via effective potentials inferred from classical molecular dynamics (MD) trajectories based on a well-established all-atom potential function. Comparisons of 10 ns long MD trajectories between the CG and the corresponding all-atom model show similar root-mean-square deviations from the canonical B-form DNA, and similar structural fluctuations. At the same time, the CG model is 10 to 100 times faster depending on the length of the DNA fragment in the simulation. Analysis of dispersion curves derived from the CG model yields longitudinal sound velocity and torsional stiffness in close agreement with the experiment. The computational efficiency of the model makes it possible to calculate thermal conductivity of a single DNA molecule not yet available experimentally. For a uniform (polyG-polyC) DNA the estimated conductivity coefficient is 0.3 W/mK which is half the value of thermal conductivity for water. This result is in stark contrast with estimates of thermal conductivity for simplified, effectively 1D chains ("beads on a spring") that predict anomalous (infinite) thermal conductivity. Thus, full 3D character of DNA double-helix retained in the proposed model appears to be essential for describing its thermal properties at a single molecule level.

I. INTRODUCTION

Heat conductivity in nanostructures is of great importance both from fundamental and applied points of view. For example, superior thermal conductivity has been observed in graphene [1, 2] and carbon nanotube [3], which has raised an exciting prospect of using these materials in thermal devices [4–8]. Generally, one can not expect that bulk thermal properties of a material will remain unchanged at nanoscale: in some nano materials such as silicon thermal conductivity is about two orders of magnitude smaller than that of bulk crystals [9], with the reduction in conductivity attributed to strong inelastic surface scattering. Furthermore, familiar physical laws such as Fourier law of heat transfer that work in bulk materials are no longer valid on the nanoscale [10–13].

Deoxyribonucleic acid (DNA) is one of the most promising nanowire materials due to the relative ease of modifications combined with the self-assembly capability which make it possible to construct a great variety of DNA-based nanostructures [14, 15]. While electrical conductivity of single DNA molecules has been extensively studied, the corresponding thermal properties remain largely unexplored. The first attempt to measure thermal conductivity of DNA-gold composite [16] gave an estimate of 150 W/mK for the coefficient of thermal conductivity, which was conspicuously close to that of pure gold. The study concluded that molecular vibrations play a key role in thermal conduction process in DNA molecule, but thermal conductivity of single molecule DNA remained unknown.

At the same time, theoretical approaches to the problem have met with their own difficulties. Numerical modeling of heat transfer along carbon nanotubes and nanoribbons showed that thermal conductivity increases steadily with the length of the specimen [10–13]. If one makes an analogy with 1D unharmonic chains that always have infinite thermal conductivity [17, 18], one might interpret these results as suggesting anomalously high thermal conductivity for quasi one-dimensional nanosystems. Since at some level the DNA double helix may also be considered as a quasi 1D system, one

wonders if the corresponding thermal conductivity is also anomalously high, increasing with the length of the DNA molecule? But it may also be that the over-simplified "beads on a spring" description of the DNA is inappropriate in this context, and thermal properties of the double helix do not show the low dimensional anomaly.

The goal of this work is to address this issue by direct modeling of heat transfer along the DNA double helix via coarse-grained description, based on classical molecular dynamics of the DNA, that retains key properties of the fully atomistic picture of the molecule.

Classical molecular dynamics (MD) simulations based on fully atomistic (all-atom) representations [19–21] are among the most widely used tools currently employed to study dynamics of the DNA double helix [22]. In these simulations the dynamics of the atoms is governed by semi-empirical potentials, or force-fields; CHARMM27 [20, 21] or AMBER [23] are the most common force-fields that accurately reproduce a variety of structural and dynamical properties of small fragments of canonical and non-canonical nucleic acids in water, at least on time-scales of up to one microsecond [22, 24–32]. Importantly, classical force-fields such as AMBER [33] can reproduce high-level quantum mechanical calculations for hydrogen bonding and base stacking interactions [34, 35]. However, accuracy of these all-atom models in which every atom of the DNA fragment and all of the surrounding solvent molecules are represented explicitly comes at a price of substantial computational expense that limits the range of applicability of the models.

The so-called *implicit solvent approach* [36–40] reduces the computational expense by replacing the discrete water environment with a continuum with dielectric and "hydrophobic" properties of water. However, even in this case all-atom simulations may be computationally expensive. For example, a 5 ns long simulation of a 147 base pair DNA fragment reported in Ref. [41] took 115 hours on 128 processors. This example suggests that all-atom models may not be suitable for the program set out in this work, in which heat transfer along long fragments of DNA will have to be examined. We therefore

resort to yet another level of approximation – coarse-graining (CG), where sets of original atoms are grouped into single “united atoms” or grains.

Naturally, there is no unique prescription for subdividing a macromolecule into grains. The grouping of individual atoms into grains aims to achieve a balance between faithful representation of the underlying dynamics and the associated computational expense which is directly related to the number of grains retained in the CG description. A fairly large number of coarse-grain DNA models has been developed [42–61]. Many of these models are phenomenological, in which each nucleotide is represented by 1 to 3 grains interacting via relatively simple pair potentials designed to reproduce either certain set of experimental properties or the results of numerical simulations based on the corresponding all-atom models. However, the oversimplified description of the nitrogen bases carries the risk of losing some key details of the base-base interactions, particularly their stacking part, that affect intramolecular rearrangements. The latter plays a very important role in heat transfer along the DNA molecule [62]. To make sure the nitrogen bases are treated as accurately as possible within CG description, we followed a strategy in which each base is modeled by three grains; the interaction between the bases is modeled at the all-atom level via a computationally effective strategy described below.

The remainder of this work is organized as follows. We begin with a detailed description of the coarse-graining procedure leading to the proposed model, followed by a details of the potential function. We then validate the model by comparing its dynamics with that of the corresponding all-atom model. Small amplitude vibrations and dispersion curves are analyzed next, leading to an additional verification of the model by comparison of several predicted characteristics (speed of sound, torsional rigidity) with the experiment. Then, we describe in detail the formalism used to model the heat transfer along a single DNA molecule. In “Conclusion” we provide a summary of the results and a brief discussion.

II. THE COARSE-GRAINED MODEL OF DNA

The fine-grain to coarse-grain reduction employed by our model is shown in Fig. 1. Within the coarse-grain model we combine all of the original atoms of the phosphate and C5' groups [atoms P, O1P, O2P, O3', O5', C5'H₂, Fig. 1 (a)] into a single [P] particle which is placed at the position of the original P atom, and has mass of $m_{[P]} = 109$ a.e. We combined C5' and the phosphate groups rest on the work by Bruant et al. [42], where all-atom molecular simulations were used to identify a set of relatively rigid groups of atoms in the DNA.

The sugar groups are described by two grains which are placed on the original C3' and C1' atoms; they will be denoted as [C3] and [C1]. The grain [C3] (includes C3', C3'H and H4' atoms) has a mass of $m_{[C3]} = 26$ a.e., and [C1] (includes C1', H1', C2', H2'1, H2'2 and O4' atoms) has a mass $m_{[C1]} = 43$ a.e. Thus, within our coarse-grain model the backbone of the double helix is represented by a chain of 3 particles (grains) [P], [C3] and [C1], Fig. 1 (b).

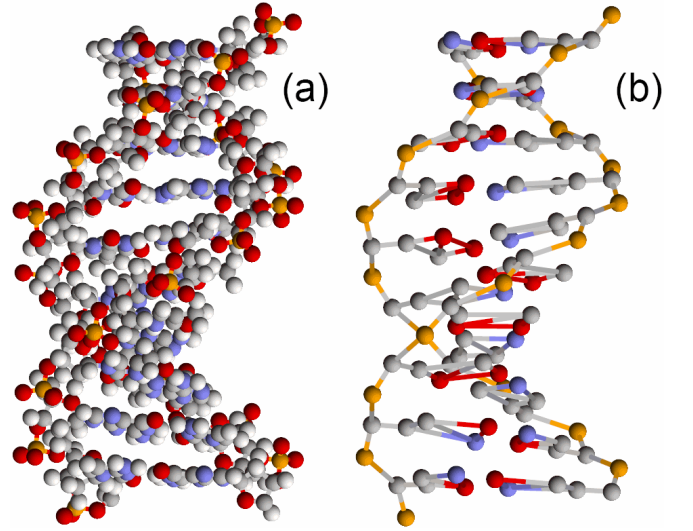


FIG. 1: View of a DNA fragment (CGTTTAAAGC) for (a) standard all-atom representation of the double helix and (b) the proposed coarse-grained model (12CG) based on 12 united atoms (grains) per base pair.

Nitrogen bases (A, T, G and C) are rather rigid, planar structures; spatial position and orientation of each base can be uniquely determined from positions of any three atoms that belong to that base. Therefore, bases A, T, G, C will be described in terms of three grains. For the A base, we identify the three grains with the original C8, N6, C2 atoms; for the T base, the three atoms are C7, O4, O2; for the G they are C8, O6, N2 atoms; and for the C base, they are C6, N4, and O2 original atoms.

Interactions between neighboring base pairs are obviously very important for heat transfer along the DNA molecule. So within the framework of our coarse-grained model the stacking of neighboring base pairs should be taken into account as accurately as possible. We take advantage of the planar structure of the bases to bring the accuracy of the stacking interactions close to the all-atom level, but with little additional computational expense: from the known grain coordinates of each coarse-grain base, one can trivially restore coordinates of all of the original atoms in the base with virtually no additional computational expense. We then calculate the stacking energy using accurate all-atom potentials, see section III for details.

The distribution of the total mass of X (X = A, T, G, C) base between its three defining grains, m_1 , m_2 , m_3 can be found from the condition of preserving the total mass ($m_1 + m_2 + m_3 = m_X$) and preserving the position of the center of mass. Values of the grain masses are shown in table I.

Thus within the suggested model one base-pair (bp) of the DNA double helix consists of 12 grains – we call the model “12CG” [see Fig. 1 (b)]. For N base-pair double helix, our system will consist of $12N$ grains having coordinates $\{\mathbf{x}_{n,i}\}_{n=1, i=1}^{N, 12}$. Here the first subscript n stands for the base-pair number, the second one i stands for the particle type: $i = 1$ for phosphate group, $i = 2$ and 3 for first and sec-

TABLE I: Masses of the three grains (m_1, m_2, m_3) for each of the base X=A, T, G, C. In units of proton mass m_p

X	m_1	m_2	m_3
A	52.230	28.139	53.632
T	51.822	16.204	56.974
G	61.731	34.357	53.912
C	39.254	35.492	35.254

ond grains of sugar ring group, $i = 4, 5, 6$ for a base of n -th site of a first strand, $i = 7$ and 8 for first and second grains of sugar ring group, $i = 12$ for a phosphate group, $i = 9, 10, 11$ for a base of n -th site of a second strand. Note that within our terminology the simplest possible "beads-on-spring" model would be called "1CG" (one grain per base pair), and the all-atom representation would be "40CG", although in this case the exact number would depend slightly on the base sequence.

III. THE POTENTIAL FUNCTION

To describe the interaction between the grains, we employ a pair potential function that contains the "standard" terms used in classical molecular dynamics simulations [63, 64]. These terms include the internal energy contributions such as bond stretching and angle bending, short-range Lennard-Jones (LJ) interactions, and long-range electrostatic interactions in the presence of water and ions. The latter are modeled implicitly, at the continuum dielectric, linear response level. The detailed term by term description is given below.

The total energy of the system consists of nine terms:

$$H = E_k + E_v + E_b + E_a + E_t + E_{hb} + E_{st} + E_{el} + E_{LJ}. \quad (1)$$

The first term E_k stands for kinetic energy of the system

$$E_k = \sum_{n=1}^N \sum_{i=1}^{12} \sum_{j=1}^3 \frac{1}{2} M_i \dot{x}_{n,i,j}^2, \quad (2)$$

with first subscript n being number of the base-pair, second subscript i being the number of the grain in n -th base-pair of the double helix, the third one j being the number of the coordinate of the grain (n, i): $\mathbf{x}_{n,i} = (x_{n,i,1}, x_{n,i,2}, x_{n,i,3})$. Masses of grains are $M_1 = M_{12} = m_{[P]}$, $M_2 = M_7 = m_{[C3]}$, $M_3 = M_8 = m_{[C1]}$, $M_4 = m_{X,1}$, $M_5 = m_{X,2}$, $M_6 = m_{X,3}$, $M_9 = m_{Y,1}$, $M_{10} = m_{Y,2}$, $M_{11} = m_{Y,3}$, where X,Y denote base types A, T, G, C.

The second term E_v in the Hamiltonian (1) stands for deformation energy of "valence" (pair) bonds.

$$\begin{aligned} E_v = & \sum_n U_{PC3}(\mathbf{x}_{n,1}, \mathbf{x}_{n,2}) + U_{C3C1}(\mathbf{x}_{n,2}, \mathbf{x}_{n,3}) \\ & + U_{C3P}(\mathbf{x}_{n,2}, \mathbf{x}_{n+1,1}) + U_{PC1}(\mathbf{x}_{n,1}, \mathbf{x}_{n,3}) \\ & + U_{C1P}(\mathbf{x}_{n+1,1}, \mathbf{x}_{n,3}) + U_{PP}(\mathbf{x}_{n+1,1}, \mathbf{x}_{n,1}) \\ & + U_{PC3}(\mathbf{x}_{n,7}, \mathbf{x}_{n,12}) + U_{C3C1}(\mathbf{x}_{n,7}, \mathbf{x}_{n,8}) \\ & + U_{C3P}(\mathbf{x}_{n-1,12}, \mathbf{x}_{n,7}) + U_{PC1}(\mathbf{x}_{n,12}, \mathbf{x}_{n,8}) \\ & + U_{C1P}(\mathbf{x}_{n-1,12}, \mathbf{x}_{n,8}) + U_{PP}(\mathbf{x}_{n-1,12}, \mathbf{x}_{n,12}). \end{aligned} \quad (3)$$

TABLE II: Values of the stiffness coefficients K_{XY} and bond lengths R_{XY} for pair interaction potentials $U_{XY}(\mathbf{x}_1, \mathbf{x}_2)$ for bonds $XY = PC3, C3C1, C3P, PC1, C1P$ and PP .

XY	PC3	C3C1	C3P	PC1	C1P	PP
K_{XY} (eV/Å ²)	9.11	8.33	0.694	0.66	0.781	0.20
R_{XY} (Å)	2.6092	2.3657	4.0735	3.6745	4.8938	6.4612

Pair potentials have a form

$$U_{XY}(\mathbf{x}_1, \mathbf{x}_2) = \frac{1}{2} K_{XY} (|\mathbf{x}_2 - \mathbf{x}_1| - R_{XY})^2, \quad (4)$$

where for a $XY = PC3, C3C1, C3P, PC1, C1P, PP$ bond parameter R_{XY} is equilibrium length, parameter K_{XY} is a bond stiffness. Values of these parameters were obtained by analysis of all-atomic MD trajectories. These values are given in the table II.

The third term E_b in the Hamiltonian (1) describes base deformation energy

$$\begin{aligned} E_b = & \sum_n U_X(\mathbf{x}_{n,3}, \mathbf{x}_{n,4}, \mathbf{x}_{n,5}, \mathbf{x}_{n,6}) \\ & + U_Y(\mathbf{x}_{n,8}, \mathbf{x}_{n,9}, \mathbf{x}_{n,10}, \mathbf{x}_{n,11}). \end{aligned} \quad (5)$$

A base X (X=A, T, G, C) deformation energy is given by

$$\begin{aligned} U_X(\mathbf{x}_1, \mathbf{x}_2, \mathbf{x}_3, \mathbf{x}_4) = & \frac{1}{2} K_X [(|\mathbf{x}_1 - \mathbf{x}_2| - R_{X12})^2 \\ & + (|\mathbf{x}_1 - \mathbf{x}_4| - R_{X14})^2 + (|\mathbf{x}_2 - \mathbf{x}_3| - R_{X23})^2 \\ & + (|\mathbf{x}_2 - \mathbf{x}_4| - R_{X24})^2 + (|\mathbf{x}_3 - \mathbf{x}_4| - R_{X34})^2] \\ & + \epsilon_X (1 + \cos \theta), \end{aligned} \quad (6)$$

where θ is an angle between two planes $\mathbf{x}_1\mathbf{x}_2\mathbf{x}_4$ and $\mathbf{x}_2\mathbf{x}_3\mathbf{x}_4$ (equilibrium corresponds to all four points lying in one plane and $\theta = \pi$). Values of potential parameters can be found in the table III. Parameters R_{X14}, \dots, R_{X34} were defined as equilibrium distances between corresponding points on bases, values of parameters K_X and ϵ_X were determined from analysis of frequency spectrum of base oscillations in all atomic DNA molecular dynamics [19].

The fourth term E_a in the Hamiltonian (1) describes the energy of angle deformation

$$E_a = \sum_n \{ U_{C3PC3}(\mathbf{x}_{n-1,2}, \mathbf{x}_{n,1}, \mathbf{x}_{n,2})$$

TABLE III: Values of parameters for potential U_X describing deformation of the base X=A, T, G, C.

X	A	T	G	C
R_{X12} (Å)	2.6326	5.0291	2.5932	2.4826
R_{X14} (Å)	4.3195	2.7007	5.2651	2.6896
R_{X23} (Å)	4.2794	2.8651	4.2912	3.5882
R_{X24} (Å)	4.3111	5.5150	5.6654	3.5014
R_{X34} (Å)	3.5187	4.5399	4.5807	4.5523
K_X (eV/Å ²)	30	30	30	20
ϵ_X (eV)	100	100	150	70

$$\begin{aligned}
&+U_{C3PC3}(\mathbf{x}_{n,7}, \mathbf{x}_{n,12}, \mathbf{x}_{n+1,7}) \\
&+U_{C3C1N}(\mathbf{x}_{n,2}, \mathbf{x}_{n,3}, \mathbf{x}_{n,4}, \mathbf{x}_{n,5}, \mathbf{x}_{n,6}) \\
&+U_{C3C1N}(\mathbf{x}_{n,7}, \mathbf{x}_{n,8}, \mathbf{x}_{n,9}, \mathbf{x}_{n,10}, \mathbf{x}_{n,11}) \\
&+U_{NC1P}(\mathbf{x}_{n+1,1}, \mathbf{x}_{n,3}, \mathbf{x}_{n,4}, \mathbf{x}_{n,5}, \mathbf{x}_{n,6}) \\
&+U_{NC1P}(\mathbf{x}_{n-1,12}, \mathbf{x}_{n,8}, \mathbf{x}_{n,9}, \mathbf{x}_{n,10}, \mathbf{x}_{n,11})\}.
\end{aligned}$$

The potential U_{C3PC3} describes the energy of the angle $C3PC3$ deformation

$$U_{C3PC3}(\mathbf{x}_1, \mathbf{x}_2, \mathbf{x}_3) = \epsilon_P (\cos \theta - \cos \theta_P)^2,$$

with θ being an angle between vectors $\mathbf{x}_2 - \mathbf{x}_1$ and $\mathbf{x}_3 - \mathbf{x}_2$. Equilibrium value of the angle $\theta_P = 130.15^\circ$, deformation energy is $\epsilon_P = 0.5$ eV. Potential

$$U_{C3C1N}(\mathbf{x}_1, \mathbf{x}_2, \mathbf{x}_3, \mathbf{x}_4, \mathbf{x}_5) = \epsilon_C (\cos \theta - \cos \theta_C)^2$$

describes angle $C3'C1'Z$ deformation energy changing, where $Z = N9$ for bases A, G and $Z = N1$ for bases T, C. Equilibrium value of the angle $\theta_{C1} = 141.63^\circ$, deformation energy is $\epsilon_{C1} = 3.0$ eV. Potential

$$U_{NC1P}(\mathbf{x}_1, \mathbf{x}_2, \mathbf{x}_3, \mathbf{x}_4, \mathbf{x}_5) = \epsilon_{NCP} (\cos \theta - \cos \theta_{NCP})^2$$

describes changing of deformation energy for the angle $N9_nC1'_nP_{n+1}$ for bases A, G and the angle $N1_nC1'_nP_{n+1}$ for bases T, C. Potential $U_{NC1P}(\mathbf{x}_{n-1,12}, \mathbf{x}_{n,8}, \mathbf{x}_{n,9}, \mathbf{x}_{n,10}, \mathbf{x}_{n,11})$ describes changing of deformation energy for the angle $N9_nC1'_nP_{n-1}$ for bases A, G and angle $N1_nC1'_nP_{n-1}$ for bases T, C. In this case equilibrium value of the angle $\theta_{NCP} = 87.17^\circ$, deformation energy is $\epsilon_{NCP} = 0.3$ eV.

The fifth term E_t in the Hamiltonian (1) describes torsion deformation energy

$$\begin{aligned}
E_t = \sum_n \{ &U_{t,1}(\mathbf{x}_{n,2}, \mathbf{x}_{n,3}, \mathbf{x}_{n,4}, \mathbf{x}_{n,5}, \mathbf{x}_{n,6}) \\
&+U_{t,1}(\mathbf{x}_{n,7}, \mathbf{x}_{n,8}, \mathbf{x}_{n,9}, \mathbf{x}_{n,10}, \mathbf{x}_{n,11}) \\
&+U_{t,2}(\mathbf{x}_{n,2}, \mathbf{x}_{n+1,1}, \mathbf{x}_{n+1,2}, \mathbf{x}_{n+1,3}) \\
&+U_{t,2}(\mathbf{x}_{n+1,7}, \mathbf{x}_{n,12}, \mathbf{x}_{n,7}, \mathbf{x}_{n,8}) \\
&+U_{t,3}(\mathbf{x}_{n,3}, \mathbf{x}_{n,2}, \mathbf{x}_{n+1,1}, \mathbf{x}_{n+1,2}) \\
&+U_{t,3}(\mathbf{x}_{n,7}, \mathbf{x}_{n,12}, \mathbf{x}_{n+1,7}, \mathbf{x}_{n+1,8}) \}.
\end{aligned}$$

Potential $U_{t,1}(\mathbf{x}_{n,2}, \mathbf{x}_{n,3}, \mathbf{x}_{n,4}, \mathbf{x}_{n,5}, \mathbf{x}_{n,6})$ describes the energy of the torsion $C3'C1'N9C8$ ($C3'C1'N1C6$) – i.e. rotations of a base A, G (T, C) around the bond $C1'—N9$ ($C1'—N1$). Rotation energy is given by

$$U = \epsilon_{t,1}(1 - \cos \phi)$$

(in equilibrium the torsion equals zero), deformation energy is $\epsilon_{t,1} = 0.5$ eV.

Potentials $U_{t,2}(\mathbf{x}_{n,2}, \mathbf{x}_{n+1,1}, \mathbf{x}_{n+1,2}, \mathbf{x}_{n+1,3})$ and $U_{t,2}(\mathbf{x}_{n+1,7}, \mathbf{x}_{n,12}, \mathbf{x}_{n,7}, \mathbf{x}_{n,8})$ describe deformation energy of the torsion $C3_nP_{n+1}C3_{n+1}C1_{n+1}$

$$U_{t,2} = \epsilon_{t,2}(1 - \cos \phi \cos \phi_2 - \sin \phi \sin \phi_2).$$

Equilibrium value of the torsion is $\phi_2 = -26.21^\circ$, deformation energy is $\epsilon_{t,2} = 0.5$ eV.

Potentials $U_{t,3}(\mathbf{x}_{n,3}, \mathbf{x}_{n,2}, \mathbf{x}_{n+1,1}, \mathbf{x}_{n+1,2})$ and $U_{t,3}(\mathbf{x}_{n,7}, \mathbf{x}_{n,12}, \mathbf{x}_{n+1,7}, \mathbf{x}_{n+1,8})$ describe deformation energy of the torsion $C1_nC3_nP_{n+1}C3_{n+1}$

$$U_{t,3} = \epsilon_{t,3}(1 - \cos \phi \cos \phi_3 - \sin \phi \sin \phi_3).$$

Equilibrium value of the torsion is $\phi_3 = 48.58^\circ$, deformation energy is $\epsilon_{t,3} = 0.5$ eV.

The sixth term E_{hb} in the Hamiltonian (1) describes the energy of hydrogen bonds between complementary bases. Since each nitrogen base is a rigid planar structure, one can restore positions of all its original atoms from positions of the three coarse-grain atoms, as outlined in the previous section. Hence we can use interaction potentials from the all-atom AMBER potential [19] for description of hydrogen bonds and stacking interactions. Thus

$$E_{hb} = \sum_n V_{XY}(\mathbf{x}_{n,4}, \mathbf{x}_{n,5}, \mathbf{x}_{n,6}, \mathbf{x}_{n,9}, \mathbf{x}_{n,10}, \mathbf{x}_{n,11}),$$

where $V_{XY}(\mathbf{x}_1, \mathbf{x}_2, \mathbf{x}_3, \mathbf{x}_4, \mathbf{x}_5, \mathbf{x}_6)$ is a potential of interaction between X (X=A,T,G,C) base, whose position is defined by three points $\mathbf{x}_1, \mathbf{x}_2, \mathbf{x}_3$ and Y (Y=A,T,G,C) base, whose position is defined by three points $\mathbf{x}_4, \mathbf{x}_5, \mathbf{x}_6$.

The main part of the hydrogen bond energy is interactions between atoms neighboring to the hydrogen bond – see Fig. 2 (a) and (b). Hence the number of interacting atoms can be decreased. Let's denote this “reduced” potential by $V_{XY}^*(\mathbf{x}_1, \mathbf{x}_2, \mathbf{x}_3, \mathbf{x}_4, \mathbf{x}_5, \mathbf{x}_6)$. Then

$$E_{hb} = \sum_n V_{XY}^*(\mathbf{x}_{n,4}, \mathbf{x}_{n,5}, \mathbf{x}_{n,6}, \mathbf{x}_{n,9}, \mathbf{x}_{n,10}, \mathbf{x}_{n,11}).$$

Neighboring base pairs interaction energy is given by

$$\begin{aligned}
E_{st} = \sum_n \{ &V_{XY}(\mathbf{x}_{n,4}, \mathbf{x}_{n,5}, \mathbf{x}_{n,6}, \mathbf{x}_{n+1,4}, \mathbf{x}_{n+1,5}, \mathbf{x}_{n+1,6}) \\
&+V_{XY}^*(\mathbf{x}_{n,4}, \mathbf{x}_{n,5}, \mathbf{x}_{n,6}, \mathbf{x}_{n+1,9}, \mathbf{x}_{n+1,10}, \mathbf{x}_{n+1,11}) \\
&+V_{XY}(\mathbf{x}_{n,9}, \mathbf{x}_{n,10}, \mathbf{x}_{n,11}, \mathbf{x}_{n+1,9}, \mathbf{x}_{n+1,10}, \mathbf{x}_{n+1,11}) \\
&+V_{XY}^*(\mathbf{x}_{n,9}, \mathbf{x}_{n,10}, \mathbf{x}_{n,11}, \mathbf{x}_{n+1,4}, \mathbf{x}_{n+1,5}, \mathbf{x}_{n+1,6}) \}.
\end{aligned}$$

Atoms whose interactions are taken into account in calculation of neighboring base pair interaction energy, are shown on the Fig. 2 (c).

The eighth term E_{el} of the Hamiltonian (1) describes the charge-charge interactions within the double helix. Within our model, only the phosphate groups interact via long-range electrostatic forces. We assume that each [P] grain has charge equal to the electron charge $q_P = -1e$, while all other particle are assigned zero charge. The total electrostatic energy of the DNA in aqueous environment (including ions) is written as $E_{el} = E_{vac} + \Delta G_{solv}$, where E_{vac} represents the Coulomb interaction energy in vacuum, and ΔG_{solv} is defined as the free energy of transferring the molecule from vacuum into solvent, i.e. solvation free energy. The above decomposition is an approximation made by most classical (non-polarizable) force-fields. Within our model we further assume

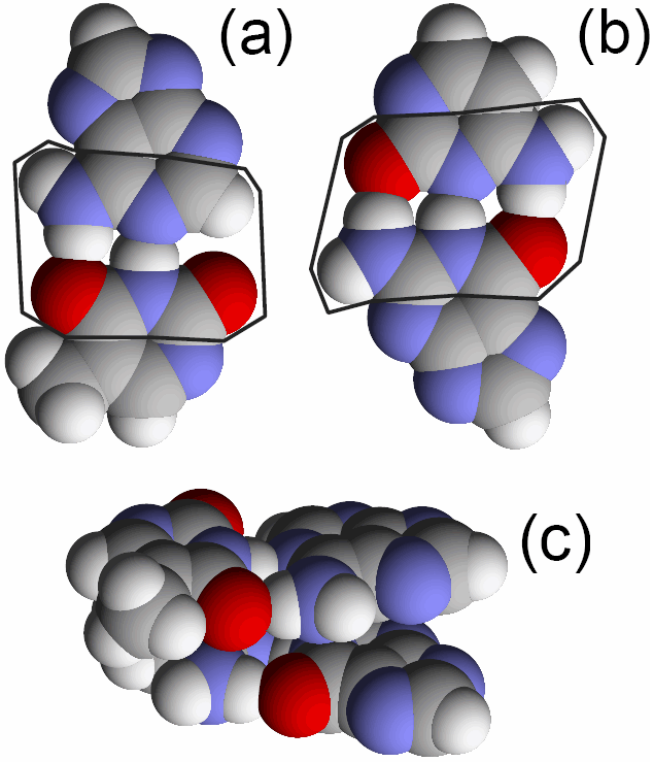


FIG. 2: View of (a) AT base pair, (b) GC base pair (highlighted are atoms which constitute mostly to base interaction energy) and (c) two neighboring base pairs (AT and GC).

that ΔG_{solv} contains only the electrostatic part; this is reasonable assumption as long as the shape of the DNA double-helix does not change drastically during the dynamics (e.g. the strands do not separate), and thus changes in the “hydrophobic” part of ΔG_{solv} can be neglected. While the computation of the Coulomb part of the interaction is trivial, estimation of ΔG_{solv} is not, due to non-trivial shape of the biomolecule. Within the framework of the continuum dielectric, linear response theory the principal way of estimating ΔG_{solv} is solving the Poisson-Boltzmann (PB) equation with the boundary conditions determined by the molecular surface that separates the high dielectric solvent from the low dielectric interior of the molecule. However, the corresponding procedures are expensive, and currently of limited practical use in dynamical simulations. We therefore resort to the so-called generalized Born model [65–67] (GB), which is the most widely used alternative to the PB treatment when speed of computation is a concern, particularly in molecular dynamics [36], including simulations of nucleic acids [41, 68–77].

The GB model approximates ΔG_{solv} by the following formula proposed by Still et al. [65]

$$\Delta G_{solv} \approx -\frac{1}{2} \left(1 - \frac{1}{\epsilon_{out}}\right) \sum_{ij} \frac{q_i q_j}{f(r_{ij}, R_i, R_j)}, \quad (7)$$

where ϵ_{out} is the dielectric constant of water, r_{ij} is the distance between atoms i and j , q_i is the partial charge of atom i , R_i is the so-called *effective Born radius* of atom i , and

$f = \left[r_{ij}^2 + R_i R_j \exp(-r_{ij}^2 / 4 R_i R_j) \right]^{\frac{1}{2}}$. The empirical function is designed to interpolate between the limits of large $r_{ij} \gg \sqrt{R_i R_j}$ where the Coulomb law applies, and the opposite limit where the two atomic spheres fuse into one, restoring the famous Born formula for solvation energy of a single ion. The effective Born radius of an atom represents its degree of burial within the low dielectric interior of the molecule: the further away is the atom from the solvent, the larger is its effective radius. In our model, we assume constant effective Born radii which we calculate once from the first principles [78]. The screening effects of monovalent salt are introduced approximately, at the Debye-Huckel level by substitution

$$1 - \epsilon_{out}^{-1} \rightarrow 1 - \epsilon_{out}^{-1} \exp(-0.73 \kappa f).$$

The 0.73 pre-factor was found empirically to give the best agreement with the numerical PB treatment [79]. Here κ is the Debye-Huckel screening parameter $\kappa [\text{\AA}^{-1}] \approx 0.316 \sqrt{[\text{salt}] [\text{mol/L}]}$.

Further simplifications come from the fact that we have only one non-zero charge species in our model, the [P] grain. Then, the total electrostatics energy is given by

$$E_{el} = C_0 + \sum_{n=1}^N \sum_{k=1}^N V_q(\mathbf{x}_{n,1}, \mathbf{x}_{k,12}) + \sum_{n=1}^{N-1} \sum_{k=n+1}^N [V_q(\mathbf{x}_{n,1}, \mathbf{x}_{k,1}) + V_q(\mathbf{x}_{n,12}, \mathbf{x}_{k,12})].$$

where

$$V_q(\mathbf{u}_1, \mathbf{u}_2) = C_1 \left[\frac{1}{r} - \frac{1}{f(r)} \left(1 - \epsilon_{out}^{-1} e^{-0.73 \kappa f(r)} \right) \right] \quad (8)$$

Here $r = |\mathbf{u}_2 - \mathbf{u}_1|$ denotes the distance between coarse-grain [P] particles, $R_i = R_j = R_P = 2.104 \text{ \AA}$ is the effective Born radius of phosphate particle. The coefficient $C_1 = 14.400611 \text{ \AA eV}$, $\epsilon_{out} = 78$, $\kappa = 0.1$. Parameter

$$C_0 = -\frac{1}{2} C_1 \left(1 - \frac{1}{\epsilon_{out}} \right) \sum_{i=0}^N \frac{1}{R_P}$$

describes self-energy (solvation energy) of phosphate groups.

The resulting total electrostatic potential due to a single [P] particle as a function of distance is shown in Fig. 3. One can see that for small distances $r < 80 \text{ \AA}$ potential decreases with increasing distance r as r^{-3} . For long distances the fall off is exponential. Thus we can introduce a cut-off distance $R_Q = 100 \text{ \AA}$ for the electrostatics interactions. For $r > R_Q$ interaction between particles is set to zero: $V_q = 0$.

The last term E_{LJ} in the Hamiltonian (1)

$$E_{LJ} = \sum_{n=1}^N \sum_{k=1}^N [U_{11}(\mathbf{x}_{n,1}, \mathbf{x}_{k,12}) + U_{12}(\mathbf{x}_{n,1}, \mathbf{x}_{k,7}) + U_{12}(\mathbf{x}_{n,2}, \mathbf{x}_{k,12}) + U_{22}(\mathbf{x}_{n,2}, \mathbf{x}_{k,7})]$$

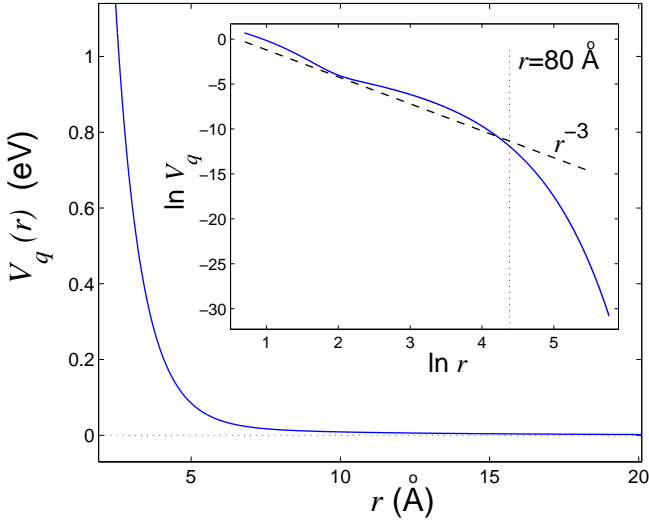


FIG. 3: Electrostatics potential $V_q(r)$, equation (8).

describes Lennard-Jones interaction between different side chain grains. Potential is given by

$$U_{ij}(\mathbf{x}_1, \mathbf{x}_2) = \epsilon_{ij} \left[\left(\frac{\sigma_{ij}}{r - d_{ij}} \right)^6 - 1 \right]^2 - \epsilon_{ij}, \quad i, j = 1, 2,$$

where $r = |\mathbf{x}_2 - \mathbf{x}_1|$ is a distance between two grains, interaction energy is $\epsilon_{ij} = \sqrt{\epsilon_i \epsilon_j}$, $d_{ij} = d_i + d_j$, $\sigma_{ij} = \sigma_i + \sigma_j$, energy parameters are $\epsilon_1 = 0.01\text{eV}$, $\epsilon_2 = 0.005\text{eV}$, diameters are $d_1 = 2.4\text{\AA}$, $d_2 = 2\text{\AA}$, parameter $\sigma_1 = 1.6\text{\AA}$, $\sigma_2 = 1.9\text{\AA}$.

IV. VALIDATION OF THE MODEL

We begin validating the proposed coarse-grain model by comparing the resulting DNA dynamics with that produced by the corresponding established all-atom model. Later in this work we will also discuss direct comparisons with the experiment (estimated sound velocities).

The constant temperature dynamics of the double helix is obtained by integrating numerically the following system of Langevin's equations:

$$\mathbf{M}_n \ddot{\mathbf{u}}_n = -\partial H / \partial \mathbf{u}_n - \Gamma \mathbf{M}_n \dot{\mathbf{u}}_n + \Xi_n, \quad (9)$$

where $n = 1, 2, \dots, N$, $\Gamma = 1/t_r$ is the Langevin collision frequency with $t_r = 1$ ps being the corresponding particle relaxation time, $\mathbf{u}_n = \{\mathbf{x}_{n,j}\}_{j=1}^{12}$ is the 36-dimensional coordinate vector of grains of the n -th base-pair of the double helix, \mathbf{M}_n is a diagonal matrix of n -th grain masses, and $\Xi_n = \{\xi_{n,k}\}_{k=1}^{36}$ is a 36-dimensional vector of Gaussian distributed stochastic forces describing the interaction of n -th base-pair grains with the thermostat with correlation functions

$$\langle \xi_{n,i}(t_1) \xi_{m,j}(t_2) \rangle = 2Mk_B T \delta_{nm} \delta_{ij} \delta(t_2 - t_1),$$

where the mass $M = M_k$, if $i = 3(k-1) + l$, $k = 1, \dots, 12$, $l = 1, 2, 3$.

To bring the temperature of the molecule to the desired value $T = 300\text{K}$, we integrate the system (9) over time $t = 20t_r$ starting from the following initial conditions

$$\{\mathbf{u}_n(0) = \mathbf{u}_n^0, \quad \dot{\mathbf{u}}_n(0) = \mathbf{0}\}_{n=1}^N \quad (10)$$

which correspond to the equilibrium state of the double helix $\{\mathbf{u}_n^0\}_{n=1}^N$. Once the system is thermalized, the temperature is maintained at $T = 300\text{K}$ and the trajectory continues for 10 ns.

The first step in the validation procedure is to estimate Root-mean square deviation (RMSd) of the end point ($t=10$ ns) of the trajectory from a reference DNA structure, and compare the RMSd values between the CG and the reference all-atom trajectory (AMBER). Given two structures, the RMSd can be computed as:

$$d = \left[\frac{1}{12N} \min_{\mathbf{s} \in SO(3), \mathbf{l} \in \mathbb{R}^3} \sum_{i=1}^{12N} \left(\mathbf{r}^i - (\mathbf{S} \mathbf{r}'^i + \mathbf{l}) \right)^2 \right]^{1/2},$$

where $\mathbf{r}^i, i = 1, \dots, 12N$ is the reference (e.g. initial), and \mathbf{r}'^i is the final set of coordinates of the structure. The expression is minimized over a translation (vector \mathbf{l}) and a rotation around a fixed point (operator \mathbf{S}). The details of the algorithm are described in the Ref. [80]. Analysis of RMS deviations from reference structures as a function of simulation time is commonly used as initial check of stability of the system and quality of the underlying models [66, 68].

As is common in the field, the following sequence of 12 base pairs d(CGCGAATTGCGC)₂ (Dickerson's dodecamer) was used for this test. A constant temperature ($T = 300\text{K}$) simulation was performed for 10 ns. As one can see from the Fig. 4 the various RMSd metrics fluctuate around their equilibrium values, which suggests that the system remains stable in dynamics, on the time scale of the simulation. A comparison with the corresponding all-atom simulation is shown in Fig. 4(b). This all-atom simulation uses the same 12 base-pair fragment, and is based on the latest nucleic acid force-field (parmbsc0 [23]) from AMBER. The solvent was represented via the generalized Born implicit solvent approximation; all other parameters such as Langevin collision frequency, ambient salt concentration, etc. were the same as in the CG simulation shown in Fig. 4(a). Comparing Figs. 4(a) and (b) we can see that the all-atom RMSd is slightly larger than that of the 12CG models. We can conclude that the 12CG model is somewhat more rigid as compared with all-atom one. Finally, we note that the equilibrium RMS deviation from the experimental (X-ray) B-form DNA is about 2.5\AA , Fig. 4(c), which is similar to what was observed earlier in all-atom implicit solvent simulations [68].

Another common set of structural parameters used in validation of DNA models is helical parameters. These parameters determine the interaction between neighboring base pairs, hence they are significant for heat transfer processes. Let's choose, for simplicity, two of them which are the most relevant ones for describing the over-all structure of the double helix. The first of these parameters is the angle ϕ , called *twist*, through which each successive base pair is rotated around the

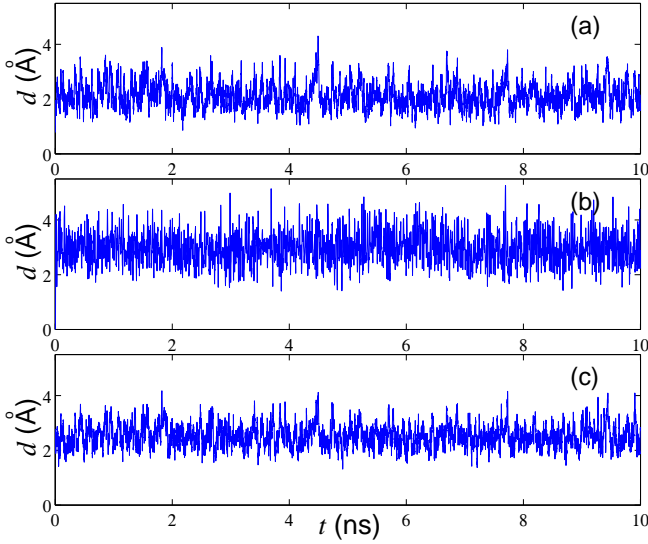


FIG. 4: Comparison of time dependence of RMS deviation relative to various reference structures in coarse-grained and all-atom molecular dynamics simulations of a 12 base-pair DNA fragment at $T=300\text{K}$. (a) 12CG model simulation. RMSd is relative to the first frame. (b) All-atom model simulation. RMSd is relative to the first frame, (c) 12CG model simulation. RMSd is relative to B-DNA X-ray structure [81]. For all-atom structures the RMSd is computed only for the subset of atoms that define grain centers in the corresponding CG model.

helical axis relative to its (nearest neighbor) predecessor. The second one, *rise*, is the distance between such two neighboring base pairs. Given the structure of a single base-pair and the values of the twist and rise, one can re-construct the whole molecule assuming that it is “one-dimensional” uniform crystal. Exact algorithm of calculating these parameters is described in [82]. We used X3DNA [82] package and in-house software for computing these parameters in our all-atom and CG models. With regards to twist and rise, the validation of our 12CG model was performed in the same manner as previously described in the context of an all-atom model [66]. The results are presented in Fig. 5, where the averages of the 10ns simulation trajectories and the standard deviations (indicated by error bars) for each base pair step are shown. One can see that the twist and rise values for 12CG model are rather close to those of the all-atom model. A small difference is comparable with that seen between DNA simulations in explicit vs. implicit solvent [66].

V. DISPERSION CURVES AND SMALL-AMPLITUDE OSCILLATIONS

The suggested 12CG model enables to compute dynamical evolution of a DNA molecule with any sequence. However, for homogeneous molecules, that is if all base pairs are identical, the molecule can be considered as quasi-one-dimensional crystal with the elementary cell being one base-pair of the double helix. This is a very useful simplification that will

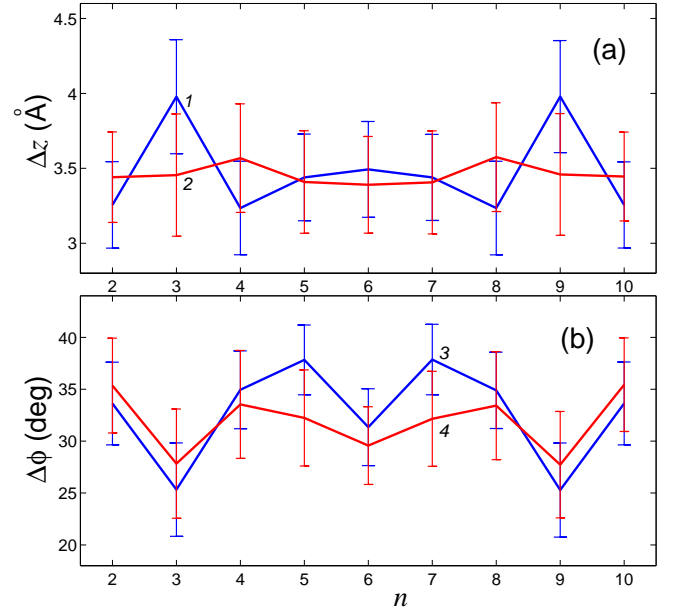


FIG. 5: Comparison of two common helical parameters (a) Δz (rise) and (b) $\Delta\phi$ (twist) between the CG model (curves 1, 3) and the corresponding all-atom model (curves 2, 4) (n – number of base pair step). Shown are averages over the corresponding 10ns molecular dynamics trajectories at $T=300\text{K}$.

be employed here; it is also a very reasonable one as long as the focus is on the over-all physics of the structure, not on sequence dependent effects. The main advantage of the assumption is that linear oscillations can be analyzed by standard techniques of solid state physics. To be specific, let’s consider a polyG double helix chain, assumed to extend along the z -axis. In the ground state of the double helix, each successive base-pair is obtained from its predecessor by translation along the z -axis by step Δz and by rotation around the same axis through helical step $\Delta\phi$. These are the rise and twist parameters introduced in the previous section.

$$\begin{aligned} x_{n,j,1} &= x_{n-1,j,1} \cos(\Delta\phi) - x_{n-1,j,2} \sin(\Delta\phi), \\ x_{n,j,2} &= x_{n-1,j,1} \sin(\Delta\phi) + x_{n-1,j,2} \cos(\Delta\phi), \\ x_{n,j,3} &= x_{n-1,j,3} + \Delta z \end{aligned} \quad (11)$$

Thus, the energy of the ground state is a function of 38 variables: $\{\mathbf{x}_{1,j}\}_{j=1}^{12}$, $\Delta\phi$, Δz , where $\mathbf{x}_{1,j} = (x_{1,j,1}, x_{1,j,2}, x_{1,j,3})$ is a radius-vector of j -th grain of the first base-pair.

Finding the ground state amounts to the following minimization problem:

$$E_0 = E_v + \dots + E_{LJ} \rightarrow \min : \{\mathbf{x}_{1,j}\}_{j=1}^{12}, \Delta\phi, \Delta z, \quad (12)$$

where the sum extends over one base-pair $n = 1$, and the relation (11) holds for calculation of the energies E_v, \dots, E_{LJ} .

Numerical solution of the problem (12) has shown that the ground state of polyG DNA corresponds to the twist value of $\Delta\phi_0 = 38.30^\circ$, and the rise value (z -step) of $\Delta z_0 = 3.339\text{\AA}$. It should be noticed that if all of the long-range interaction

were omitted, *i.e.* without two last terms E_q and E_{LJ} in the Hamiltonian (1), the helical step values would change only slightly, by 1 per cent: $\Delta\phi_0 = 38.03^\circ$, $\Delta z_0 = 3.309\text{\AA}$. Thus, long-range electrostatic interaction between the charged group results in the relative elongation of the chain by only about 1 per cent. Parameters of the double helix computed within our model differ only weakly from the “canonical” parameters of the B-conformation of a (heterogeneous) DNA double helix in the crystal form [83], for which the average twist angle is $\Delta\phi = 34^\circ \div 36^\circ$, and average rise per base pair is $\Delta z = 3.4\text{\AA}$.

To find the ground state of the homogeneous double helix under tension, it is necessary to minimize (12) under the fixed value of longitudinal step Δz . As a result, one can obtain the dependence of the homogeneous state energy on the longitudinal step. This function $E_0(\Delta z)$ has a minimum when $\Delta z = \Delta z_0$, which corresponds to the B-conformation of the double helix. Longitudinal stiffness of the helix $K_z = d^2 E_0 / d\Delta z^2|_{\Delta z_0}$. Specifically, within our model we estimate $K_z = 16 \text{ N/m}$. Since the energy E_0 which is being derived is normalized to one base pair one can calculate the stretching modulus $S = K_z \Delta z_0 = 16 \text{ N/m} \times 3.4 \text{\AA} = 5440 \text{ pN}$. This estimate is somewhat higher than the corresponding estimate of $1530 \div 3760 \text{ pN}$ obtained from fluctuations of distances between basepairs observed in MD simulations[42]. The relatively larger value of K_z from our CG model is consistent with the model’s over-all larger stiffness relative to the all-atom one, see a discussion above. Some of the difference between the two estimates may also be due to methodological differences in estimating longitudinal stiffness. Values of the stretching modulus derived from experiments are of the order 1000 pN [84–86], *i.e.* about 5 times smaller than our estimate based on the CG model. One should keep in mind, however, that we have obtained only an upper estimate for the stretching modulus: temperature was assumed to be zero, the calculations were based on a homogeneous polyG-polyC sequence that was reported to be more rigid than inhomogeneous and polyA-polyT sequences used in the experiments[87, 88], and the entropy component was not considered in our calculations.

To obtain $E_0(\Delta\phi)$, that is the dependence of the helix energy on the helical step $\Delta\phi$, we set $\Delta z \equiv \Delta z_0$ in (12) and perform the minimization with respect to the remaining 36 parameters. Then it is possible to find the torsion stiffness of the double helix $K_\phi = \Delta z_0 d^2 E_0 / d\Delta\phi^2|_{\Delta\phi_0}$. Our estimate, $K_\phi = 5.8 \times 10^{-28} \text{ J}\cdot\text{m}$, is in good agreement with the experimental value of $K_\phi = 4.1 \pm 0.3 \times 10^{-28} \text{ J}\cdot\text{m}$, obtained for DNA macromolecule in B-conformation [89].

For analysis of small-amplitude oscillations of the double helix it is convenient to use local cylindrical coordinates $\mathbf{v}_{n,j} = (v_{n,j,1}, v_{n,j,2}, v_{n,j,3})$, given by the following expressions:

$$\begin{aligned} x_{n,j,1} &= x_{n,j,1}^0 - v_{n,j,1} \sin \phi_{n,j} + v_{n,j,2} \cos \phi_{n,j}, \\ x_{n,j,2} &= x_{n,j,2}^0 + v_{n,j,1} \cos \phi_{n,j} + v_{n,j,2} \sin \phi_{n,j}, \\ x_{n,j,3} &= x_{n,j,3}^0 + v_{n,j,3}, \end{aligned} \quad (13)$$

with $\mathbf{x}_{n,j}^0$ ($n = 0, \pm 1, \pm 2, \dots; j = 1, 2, \dots, 12$) being coordinates of the grains in the ground state of the double helix,

and $\phi_{n,j}$ being angular coordinate of the grain (n, j) . Within these new coordinates the molecule’s Hamiltonian (1) has the following form:

$$H = \sum_n \left[\frac{1}{2} (\mathbf{M} \dot{\mathbf{v}}_n, \dot{\mathbf{v}}_n) + P(\mathbf{v}_{n-1}, \mathbf{v}_n, \mathbf{v}_{n+1}) \right], \quad (14)$$

where $\mathbf{v}_n = (\mathbf{u}_{n,1}, \mathbf{u}_{n,2}, \dots, \mathbf{u}_{n,12})$ is a 36-dimensional vector, \mathbf{M} is 36-dimensional diagonal mass matrix. Note that the last two terms E_q and E_{LJ} , responsible for long-range interaction, have been omitted. This simplification is critical from the methodological point of view, but has very little impact on the accuracy of the estimates of DNA thermal conductivity. The point will be discussed below.

Hamiltonian (14) corresponds to the following system of equations of motion:

$$\begin{aligned} -\mathbf{M} \ddot{\mathbf{v}}_n &= P_1(\mathbf{v}_n, \mathbf{v}_{n+1}, \mathbf{v}_{n+2}) \\ &+ P_2(\mathbf{v}_{n-1}, \mathbf{v}_n, \mathbf{v}_{n+1}) + P_3(\mathbf{v}_{n-2}, \mathbf{v}_{n-1}, \mathbf{v}_n), \end{aligned} \quad (15)$$

where $P_i(\mathbf{v}_1, \mathbf{v}_2, \mathbf{v}_3) = \partial P / \partial \mathbf{v}_i$, $i = 1, 2, 3$. Within the linear approximation, the system (15) has the form

$$-\mathbf{M} \ddot{\mathbf{v}}_n = B_1 \mathbf{v}_n + B_2 \mathbf{v}_{n+1} + B_2^* \mathbf{v}_{n-1} + B_3 \mathbf{v}_{n+2} + B_3^* \mathbf{v}_{n-2}, \quad (16)$$

where matrix elements are given by

$$B_1 = P_{11} + P_{22} + P_{33}, \quad B_2 = P_{12} + P_{23}, \quad B_3 = P_{13},$$

and partial derivative matrix is given by

$$P_{ij} = \frac{\partial^2 P}{\partial \mathbf{v}_i \partial \mathbf{v}_j}(\mathbf{0}, \mathbf{0}, \mathbf{0}), \quad i, j = 1, 2, 3.$$

Solution of the system of linear equations (16) can be found in the standard form

$$\mathbf{v}_n = A \mathbf{e} \exp[i(qn - \omega t)], \quad (17)$$

where A is linear mode amplitude, \mathbf{e} is unit vector ($|\mathbf{e}| = 1$), $q \in [0, \pi]$ is dimensionless wave number. Putting the expression (17) to the system (16), we arrive at the following 36-dimensional eigenvalue problem:

$$\begin{aligned} \omega^2 \mathbf{M} \mathbf{e} &= [B_1 + B_2 \exp(iq) + B_2^* \exp(-iq) \\ &+ B_3 \exp(2iq) + B_3^* \exp(-2iq)] \mathbf{e}. \end{aligned} \quad (18)$$

Thus to obtain dispersion relations which characterize eigenmodes of the DNA double helix one has to find all eigenvalues of the problem (18) for each value of wave number $0 \leq q \leq \pi$. Obtained dispersion curve includes 36 branches $\{\omega_j(q)\}_{j=1}^{36}$ and is shown on the Fig. 6.

It can be seen from Fig. 6 that frequency spectrum consists of low-frequency $0 \leq \omega \leq 175 \text{ cm}^{-1}$ and high-frequency $\omega \in [267, 749] \text{ cm}^{-1}$ domains. The high-frequency domain describes internal oscillations of bases. As shown in Fig. 6 (a), corresponding dispersion curves have very small slope, meaning that the high-frequency oscillations have a small dispersion. The low-frequency oscillations have larger dispersion – see Fig. 6 (b). There are two acoustic dispersion curves

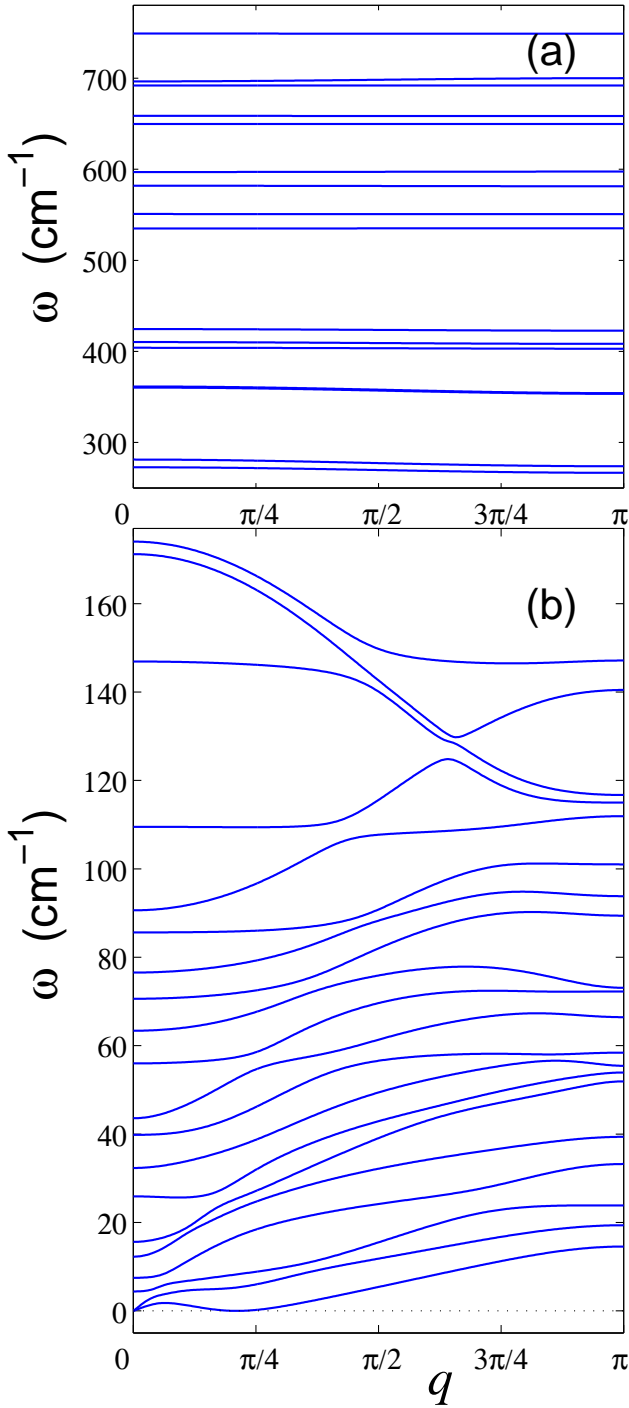


FIG. 6: 36 branches of the dispersion curve of homogeneous polyG DNA: (a) high-frequency and (b) low-frequency branches.

which include zero point ($q = 0, \omega = 0$). The first curve $\omega_1(q)$ describes torsional acoustic oscillations, the second one $\omega_2(q)$ describes longitudinal acoustic oscillations of the double helix. Thus we can obtain the two sound velocities

$$v_t = \Delta z \lim_{q \rightarrow 0} \frac{\omega_1(q)}{q}, \quad v_l = \Delta z \lim_{q \rightarrow 0} \frac{\omega_2(q)}{q},$$

with Δz being z -step of a double helix. The value of torsional

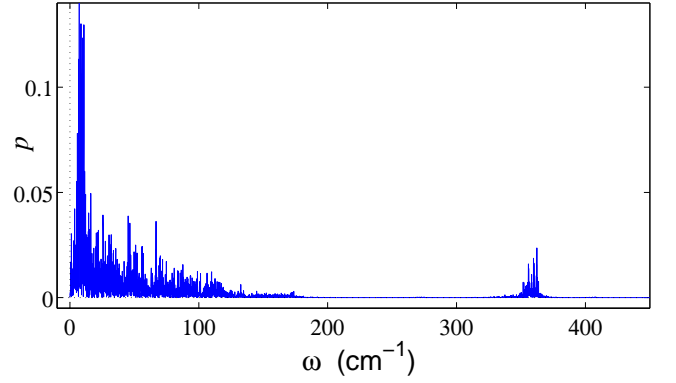


FIG. 7: Frequency spectrum density of DNA double helix thermal fluctuations at $T = 300\text{K}$.

sound velocity is $v_t = 850$ m/s, and the value of longitudinal sound velocity is $v_l = 1790$ m/s. Besides one of these dispersion curves includes the special point ($q = \Delta\phi, \omega = 0$) ($\Delta\phi$ is the angular helix step). This curve describes bending oscillations of the double helix which we do not analyze in detail because our approach neglects long-range interactions that are known to have strong effect on bending rigidity of the DNA.

The estimated longitudinal sound velocity is in agreement with an experimental value of the sound velocity in DNA fibers [90]: $v_l = 1900$ m/s. Another experimental estimate [91] of the same quantity is higher, $v_l = 2840$ m/s, and was obtained from inelastic X-ray scattering. The same work reports torsional sound velocity $v_t = 600$ m/s; the 20 % discrepancy with our estimate of $v_t = 850$ m/s appears acceptable given similar margin of error seen between different experimental estimates for the longitudinal velocity.

VI. FREQUENCY SPECTRUM OF THE THERMAL OSCILLATIONS.

Let's again consider a homogenous polyG DNA chain consisting of $N = 200$ base pairs and calculate its frequency spectrum density. We begin by simulating dynamics of the helix without taking into account long-range interactions. Later, we will turn them on to analyze the effect of making the approximation.

To obtain thermalized state of the double helix, the system of Langevin's equations (9) should be numerically integrated. For thermalization of the double helix let's consider initial conditions corresponding to the ground state (10), and integrate the system (9) for a time $t = 20t_r$. After the equilibration period, the coupling with the thermostat was switched off, frequency density $p(\omega)$ of the kinetic energy distribution was obtained. To increase precision, distribution density was calculated as an average over all grains of the helix.

Frequency spectrum density at $T = 300\text{K}$ is shown in the Fig. 7. This figure shows that without considering long-range interaction in double helix frequency density spectrum agrees well with dispersion curve branches (see Fig. 6). Frequency

spectrum is clearly divided into low-frequency $0 \leq \omega \leq 175 \text{ cm}^{-1}$ and high-frequency $267 < \omega < 749 \text{ cm}^{-1}$ intervals.

Simulating the double helix dynamics with account for all interactions (including long-range ones) yields almost the same frequency spectrum. Only the density of oscillations in the interval $0 \leq \omega < 10 \text{ cm}^{-1}$ increases.

VII. HEAT CONDUCTIVITY OF DOUBLE HELIX

For numerical modeling of the heat transfer along the DNA double helix, we consider a chain of a fixed length with the ends placed in two separate thermostats each with its own temperature. To calculate the coefficient of thermal conductivity, we have to calculate numerically the heat flux through any cross section of the double helix. Therefore, first we need to obtain a formula for the longitudinal local heat flux.

Let us consider the homogeneous double helix poly-G DNA. (The method below is also applicable to any sequences of bases).

If long-range interactions (electrostatic and van der Waals's) are not taken into account we can present the system Hamiltonian of the helix (1) in the form

$$H = \sum_n \frac{1}{2} (\mathbf{M}\dot{\mathbf{u}}_n, \dot{\mathbf{u}}_n) + P(\mathbf{u}_{n-1}, \mathbf{u}_n, \mathbf{u}_{n+1}), \quad (19)$$

where the first term describes the kinetic energy of atoms in the cell and the second term describes the energy of interaction between the atoms and with the atoms of neighboring cells. The corresponding equations of motion can be written in the form

$$\mathbf{M}\ddot{\mathbf{u}}_n = -P_1(\mathbf{u}_n, \mathbf{u}_{n+1}, \mathbf{u}_{n+2}) - P_2(\mathbf{u}_{n-1}, \mathbf{u}_n, \mathbf{u}_{n+1}) - P_3(\mathbf{u}_{n-2}, \mathbf{u}_{n-1}, \mathbf{u}_n), \quad (20)$$

where the function P_j is defined as

$$P_j = \frac{\partial}{\partial \mathbf{u}_j} P(\mathbf{u}_1, \mathbf{u}_2, \mathbf{u}_3), \quad j = 1, 2, 3.$$

To determine the energy flux through the double helix cross section, we present formula (19) in a compact form, $H = \sum_n h_n$, where h_n is the energy density,

$$h_n = \frac{1}{2} (\mathbf{M}\dot{\mathbf{u}}_n, \dot{\mathbf{u}}_n) + P(\mathbf{u}_{n-1}, \mathbf{u}_n, \mathbf{u}_{n+1}). \quad (21)$$

Local longitudinal heat flux j_n is defined through local energy density h_n by the discrete version of the continuity equation,

$$\frac{d}{dt} h_n = j_n - j_{n+1}. \quad (22)$$

Using the energy density (21) and the equations of motion (20), we can derive the following relations:

$$\begin{aligned} \frac{d}{dt} h_n &= (\mathbf{M}\ddot{\mathbf{u}}_n, \dot{\mathbf{u}}_n) + (P_{1,n}, \dot{\mathbf{u}}_{n-1}) + (P_{2,n}, \dot{\mathbf{u}}_n) \\ &+ (P_{3,n}, \dot{\mathbf{u}}_{n+1}) = -(P_{1,n+1}, \dot{\mathbf{u}}_n) - (P_{3,n-1}, \dot{\mathbf{u}}_n) \\ &+ (P_{1,n}, \dot{\mathbf{u}}_{n-1}) + (P_{3,n}, \dot{\mathbf{u}}_{n+1}), \end{aligned}$$

where

$$P_{j,n} = P_j(\mathbf{u}_{n-1}, \mathbf{u}_n, \mathbf{u}_{n+1}), \quad j = 1, 2, 3.$$

From this and (22) it follows that the energy flux through the n -th cross section has the following simple form:

$$j_n = (P_{1,n}, \dot{\mathbf{u}}_{n-1}) - (P_{3,n-1}, \dot{\mathbf{u}}_n). \quad (23)$$

Let us note that taking into account the long-range interactions would complicate this formula considerably, making the calculations virtually intractable. This is why the approximation we have made was critical.

For a direct numerical modeling of the heat transfer along the double helix, we consider a finite structure of the length $N\Delta z$ with fixed ends. We assume that the first $N_+ = 20$ segments are placed in the thermostat at temperature $T_+ = 310 \text{ K}$ and the last $N_- = 20$ segments are placed in the other thermostat at $T_- = 290 \text{ K}$. The helix dynamics is described by the following equations of motion:

$$\begin{aligned} \mathbf{M}\ddot{\mathbf{u}}_n &= -\mathbf{F}_n - \Gamma \mathbf{M}\dot{\mathbf{u}}_n + \Xi_n^+, \quad n = 1, \dots, N_+, \\ \mathbf{M}\ddot{\mathbf{u}}_n &= -\mathbf{F}_n, \quad n = N_+ + 1, \dots, N - N_-, \\ \mathbf{M}\ddot{\mathbf{u}}_n &= -\mathbf{F}_n - \Gamma \mathbf{M}\dot{\mathbf{u}}_n + \Xi_n^-, \quad n = N - N_- + 1, \dots, N, \end{aligned} \quad (24)$$

where $\mathbf{F}_n = \partial H / \partial \mathbf{u}_n$, $\Gamma = 1/t_r$ is the damping coefficient (relaxation time $t_r = 1 \text{ ps}$, and $\Xi_n^\pm = (\xi_1^\pm, \dots, \xi_{36}^\pm)$ is 36-dimensional vector of normally distributed random forces normalized by the condition

$$\langle \xi_{n,i}^\pm(t_1) \xi_{m,j}^\pm(t_2) \rangle = 2Mk_B T_\pm \delta_{nm} \delta_{ij} \delta(t_2 - t_1),$$

where the mass $M = M_k$, if $i = 3(k-1) + l$, $k = 1, \dots, 12$, $l = 1, 2, 3$.

We take the initial conditions (10) corresponding to the equilibrium state of the helix. With these initial conditions, we integrate the equations of motion (24) numerically, by employing the velocity Verlet method with step $\Delta t = 0.0005 \text{ ps}$. After integration time t_0 [this value depends on the helix length between the thermostats, $\Delta L = (N - N_+ - N_-)\Delta z$, we observe the formation of a temperature gradient and a constant heat energy flux in the central part of the helix. It is important to notice that the time t_0 can be reduced by modifying the initial distribution of the energy, *e.g.* by taking the initial condition for the system (24) as homogeneously thermalized state with the mean temperature $T = (T_+ + T_-)/2 = 300 \text{ K}$.

After the stationary heat flux is established, the temperature distribution can be found using the formula

$$T_n = \lim_{t \rightarrow \infty} \frac{1}{36k_B t} \int_0^t (\mathbf{M}\dot{\mathbf{u}}_n(\tau), \dot{\mathbf{u}}_n(\tau)) d\tau$$

and the averaged value of the energy flux along the helix

$$J_n = \lim_{t \rightarrow \infty} \frac{\Delta z}{t} \int_0^t j_n(\tau) d\tau.$$

Distributions of the local energy flux and temperature along the helix are shown in Figs. 8 (a) and (b). In the steady-state

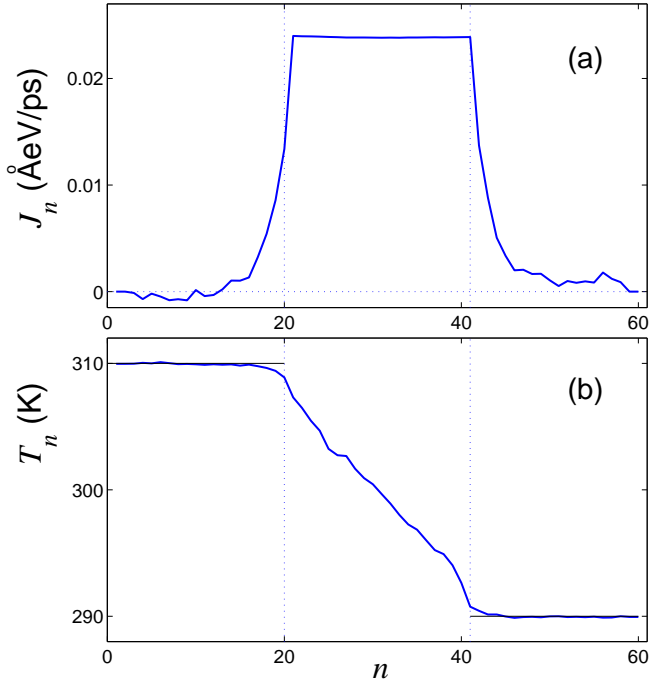


FIG. 8: Distributions of (a) local heat flux J_n and (b) local temperature T_n in the double helix with length $N\Delta z$. The parameters are $N = 60$, temperatures $T_+ = 310$ K and $T_- = 290$ K, and the number of cells in the thermostats, $N_{\pm} = 20$.

regime, the heat flux through each of the cross section at the central part of the helix should remain the same, i.e., $J_n \equiv J$, $N_+ < n \leq N - N_-$. This property can be employed as a criterion for the accuracy of numerical modeling and can also be used to determine the characteristic time for achieving the steady-state regime and calculation of J_n and T_n . Figure 8 (a) suggests that the flux is constant along the central part of the helix thus suggesting we achieved the required regime.

At the central part of the helix, we observe the linear gradient of the temperature distribution, so that we can define the coefficient of thermal conductivity as

$$\kappa(N - N_+ - N_-) = \frac{(N - N_- - N_+ - 1)J}{(T_{N_++1} - T_{N-N_-})S}, \quad (25)$$

where $S = \pi R^2$ is the area of the cross section of the double helix ($R = 8$ Å is the radius of helix on phosphorus atoms). In this way, the calculation of thermal conductivity is reduced to the calculation of the limiting value,

$$\kappa = \lim_{N \rightarrow \infty} \kappa(N).$$

In order to determine the coefficient of thermal conductivity, we need to know only the dependence of the temperature from base-pair number in the central part of the helix. However, a change of the temperature distribution at the edges of the helix can also provide some useful information. If the helix is placed into a Langevin thermostat at temperature T , each segment of the helix should have the temperature $T_n = T$ due to the energy balance of the input energy from random forces

and the energy lost to dissipation. Then, an averaged energy flow from the n -th segment of the helix can be presented as

$$\Gamma(\mathbf{M}\dot{\mathbf{u}}_n, \dot{\mathbf{u}}_n) = 36k_B T_n / t_r.$$

If only the edges of the helix are placed into thermostat, there appears an additional energy exchange with its central part, so the energy from the right edge will flow to the left one. As a result, the temperature of the left edge is reduced ($T_n \leq T_+$, $n = 1, 2, \dots, N_+$), whereas the temperature at the right edge increases ($T_n \geq T_-$, $n = N - N_- + 1, \dots, N$) – see Fig. 8 (b). This information allows us to find the energy flux in the central part of the double helix using only the energy imbalance at the edges,

$$\frac{J t_r}{\Delta z 36 k_B} = \sum_{n=1}^{N_+} (T_+ - T_n) = \sum_{n=N-N_-+1}^N (T_n - T_-). \quad (26)$$

If the lengths of the edges placed into thermostat coincide, i.e., $N_+ = N_- = N_{\pm}$, we can rewrite this formula in the following simplified form:

$$J = \frac{\Delta z 18 k_B}{t_r} \sum_{n=1}^{N_{\pm}} (T_+ - T_- - T_n + T_{N+1-n}). \quad (27)$$

Equation (26) gives an alternative way for calculating the thermal energy flux J and can be employed for verifying the results obtained by the use of Eq. (23). Let us note that although (23) is obtained under the assumption of no long-range interactions, formula (27) remains valid also if these interactions are taken into account.

Numerical modeling of the heat transfer shows that both formulas lead to the same value of the heat-conductivity coefficient if long-range interactions are absent. When $N=80$ (the number of internal links $N_i = N - N_+ - N_- = 20$), the heat-conductivity coefficient $\kappa = 0.26$ W/mK. When $N = 80$ ($N_i = 40$) – conductivity $\kappa = 0.29$ W/mK, when $N = 120$ ($N_i = 80$) – $\kappa = 0.27$ W/mK, and when $N = 200$ ($N_i = 160$) – $\kappa = 0.28$ W/mK. The same values are obtained also if the long-range interactions are taken into account (and the heat flow is calculated by formula (27) only). These considerations help us reach the conclusion that the contribution of the long-range interactions to the heat transfer along the double helix is very minor.

It is worth noting that the use of formula (27) for calculating the value of heat transfer requires more time-consuming calculations. Therefore, it is preferable to use formula (23). Also, equation (23) allows one to estimate relative contributions of various interactions into the process of heat transfer. We find that interaction between neighboring base pairs contributes 32% to the net energy flow, with the rest coming heat transfer along the two sugar-phosphate chains.

As one can see from the results, the value of heat conductivity κ in the DNA macromolecule does not depend on the length of the molecule. This is the normal thermal conductivity for which the Fourier law is valid on the nano-level as well, at least as far as the DNA is concerned. This is in contrast to earlier models of heat conduction along carbon nanotubes

and nanoribbons that predicted anomalous thermal conductivity – divergence of the coefficient of thermal conductivity with sample length[10–13]. Compared to nanotubes, the DNA double helix is much softer, which leads to strongly nonlinear behaviour at $T = 300$ K (in contrast, a nanotube, is a rigid quasi-onedimensional structure, with only weak nonlinear dynamics).

VIII. DEPENDENCE OF THE THERMAL CONDUCTIVITY ON TEMPERATURE

At $T = 300$ K the DNA double helix exhibits high-amplitude vibrations (the amplitudes can be estimated from Fig. 4 and 5). The contribution of nonlinearity to the DNA dynamics can be estimated from the temperature dependence of dimensionless heat capacity

$$c(T) = \frac{1}{36Nk_B T} \frac{d}{dT} E(T), \quad (28)$$

where $E(T) = \langle H \rangle$ is average double helix energy at temperature T . For a harmonic system dimensionless heat capacity $c(T) \equiv 1$; for the system with strong anharmonism $c(T) < 1$, and $c(T) > 1$ for weakly anharmonic systems. As seen from Fig. 9, heat capacity of the double helix equals to 1 for low temperatures ($T < 10$ K) and increases monotonously when the temperature grows. The heat capacity $c = 1.05$ at $T = 300$ K, implying weak anharmonism.

The role of nonlinearity decreases monotonously as the temperature decreases. In limiting case $T \rightarrow 0$ the double helix becomes harmonic. Therefore the DNA thermal conductivity has to increase monotonously with temperature decrease and tend to infinity when $T \rightarrow 0$. The results of our numerical modeling confirm this conclusion – see Fig. 9 (b), curve 3. At $T \searrow 0$ the heat conductivity $\kappa \nearrow \infty$.

We should mention that the temperature dependence of the thermal conductivity found above is obtained in the framework of classical molecular-dynamics model, which does not take into account quantum effects of “frozen” high-frequency oscillations (to take those into account requires substantial modifications to the model[92, 93]). In crystals at low temperatures, thermal conductivity decays monotonically when $T \rightarrow 0$. This is explained by the fact that at low temperatures the temperature dependence of thermal conductivity is defined mainly by the temperature dependence of heat capacity.

In classical mechanics, heat capacity of phonons does not depend on temperature, whereas in quantum mechanics such a dependence is defined by the formula $c(\omega, T) = k_B F_E(\omega, T)$, where the Einstein function

$$F_E(\omega, T) = \left(\frac{\hbar\omega}{k_B T} \right)^2 \frac{\exp(\hbar\omega/k_B T)}{[\exp(\hbar\omega/k_B T) - 1]^2},$$

where ω is the phonon frequency ($0 \leq F_E \leq 1$, function $F_E \searrow 0$ for $T \searrow 0$ and $F_E \nearrow 1$ for $T \nearrow \infty$).

As seen from the DNA dispersion curves $\{\omega_i(q)\}_{i=1}^{36}$, the main contribution in the heat conductivity is determined by 20 low-frequencies phonons (16 high-frequencies phonons have

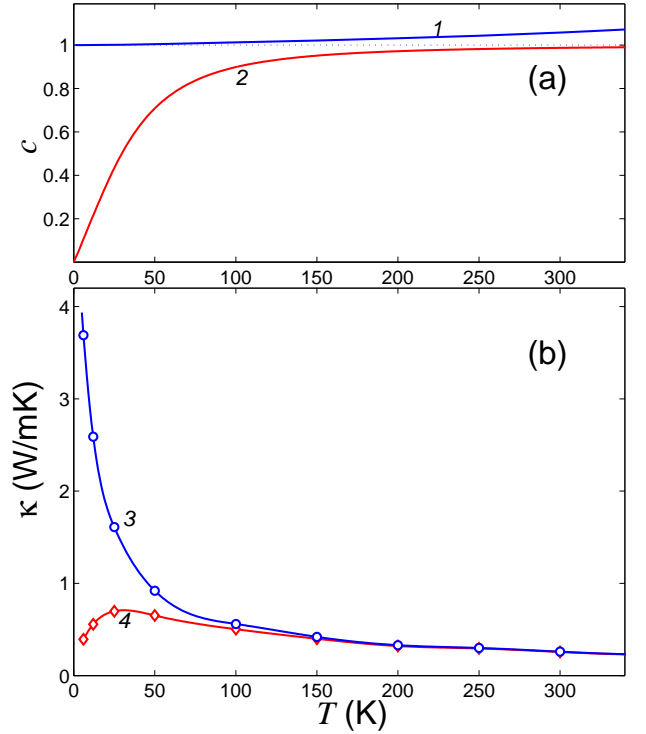


FIG. 9: (a) Temperature dependence of dimensionless specific heat $c(T)$ and $c_q(T)$ (curves 1 and 2, respectively); (b) heat conductivity $\kappa(T)$ and $\kappa_q(T)$ (curves 3 and 4, respectively) of the DNA double helix. The dependencies $c(T)$ and $\kappa(T)$ are obtained in the framework of classical molecular dynamics model, while $c_q(T)$ and $\kappa_q(T)$ are computed within the quantum framework.

very small group velocities, and therefore can not be efficient energy carriers). The temperature dependence of dimensionless heat capacity of low frequencies phonons can be found using formula

$$c_q(T) = \frac{1}{20\pi} \sum_{i=1}^{20} \int_0^\pi F_E(\omega_i(q), T) dq. \quad (29)$$

One can see from Fig. 9 that the heat capacity c_q does not noticeably depend on the temperature if $T > 150$ K, and tends monotonously to zero as the temperatures decrease below $T < 150$ K.

Thus, thermal vibrations of the double helix can be described classically for $T > 150$ K only. For lower temperatures, quantum effect caused by “freezing out” of high-frequency vibrations has to be taken into account. Due to these effects the DNA heat capacity (29) tends monotonously to zero as the temperature decreases. The double helix thermal conductivity $\kappa_q(T) \approx c_q(T)\kappa(T)$, (where the temperature dependence $\kappa(T)$ is calculated classically) because the phonon energy is proportional to heat capacity. As it seen from Fig. 9 (b) at $T > 30$ K the thermal conductivity κ_q grows monotonously as the temperature decreases, reaching its maximum at $T \approx 30$ K, and then decreases monotonously as $T \rightarrow 0$.

These calculations show that heat transfer in the DNA oc-

curs mainly due to propagation of low-frequency phonons (frequencies $\omega < 175 \text{ cm}^{-1}$), i.e. by “soft” low-frequencies waves. Such oscillations are strongly coupled to deformation of orientation angles. This fact clearly distinguishes the DNA double helix from the essentially rigid carbon nanotubes and nanoribbons. The simplest model of a one-dimensional system with orientational interaction is one-dimensional chain of interacting rotators. This chain has a finite thermal conductivity [94, 95]. On the other hand, nanotubes and nanoribbons are commonly described in the one-dimensional approximation as anharmonic Fermi Pasta Ulam (FPU) chains that lead to infinite heat conductivity [17, 18].

Thus, the double helix of a homogeneous poly-G DNA has a finite thermal conductivity $\kappa = 0.3 \text{ W/mK}$. The double helix with a nonhomogeneous (arbitrary) base sequence may be expected to have a smaller value of the heat conductivity coefficient since the presence of inhomogeneities leads to additional phonon scattering. Therefore, thermal conductivity of a generic DNA double helix, $\kappa \leq 0.3 \text{ W/mK}$, may be expected to be less than half of that of water heat conductivity which is 0.6 W/mK . This means that DNA macromolecule is a thermal insulator relative to its surrounding solution. It should be noted that measuring thermal conductivity of the DNA-gold composite structure (DNA is a matrix for gold nanoparticles) [16] gives the coefficient of thermal conductivity 150 W/mK , which is 500 times higher than the predicted thermal conductivity of pure DNA. Thus, we conclude that the measured thermal conductivity of the DNA-gold composite is completely determined by the metal component, not the DNA.

IX. CONCLUSIONS

A coarse-grain (12CG) model of DNA double helix is proposed in which each base is represented by 6 “grains”. The corresponding effective pair potentials are inferred from correlation functions obtained from classical all-atom molecular

dynamics (MD) trajectories and force-field (AMBER). The computed structural characteristics and fluctuations of the double helix at $T = 300 \text{ K}$ are in reasonable agreement with the available experimental data and earlier computations based on all-atom models. An analysis of dispersion curves derived from the CG model yields longitudinal and torsional sound velocities in close agreement with the experiment.

The numerical modeling of the heat conductivity along a single DNA molecule shows that double DNA helix has a finite (normal) thermal conductivity. This means that Fourier law is valid at nano-level for the DNA, i.e., coefficient of thermal conductivity does not depend on the length of the DNA fragment. Its thermal conductivity does not exceed 0.3 W/mK , which is two times smaller than thermal conductivity of water. Thus, the DNA double helix is a poor heat conductor. At the same time, it is known from modeling of the heat transfer along carbon nanotubes and nanoribbons that the coefficient of thermal conductivity in these systems diverges as the specimen length grows [10–13]. The anomalous behavior of thermal conductivity in long nano-objects is caused by their rigid structure as well as by their weakly nonlinear quasi one-dimensional dynamics, mostly due to rigid covalent interactions. In contrast, the DNA double-helix is a soft 3D structure with strongly nonlinear dynamics. The small value of the DNA thermal conductivity observed in our coarse-grained model strongly suggests that it captures some of the key physics of real DNA. It also leads us to conjecture that the heat conduction along the double helix is due predominantly to weak non-valent orientational interactions.

X. ACKNOWLEDGEMENTS

This research was supported by RFBR (grant 08-04-91118-a) and CRDF (grant RUB2-2920-MO-07). The authors also thank the Joint Supercomputer Center of the Russian Academy of Sciences for using their computer facilities.

-
- [1] A. A. Balandin, S. Ghosh, W. Bao, I. Calizo, D. Teweldebrhan, F. Miao, and C. N. Lau, *Nano Lett.* **8**, 902 (2008).
 - [2] S. Ghosh, I. Calizo, D. Teweldebrhan, E. P. Pokatilov, D. L. Nika, A. A. Balandin, W. Bao, F. Miao, and C. N. Lau, *Appl. Phys. Lett.* **92**, 151911 (2008).
 - [3] E. Pop, D. Mann, Q. Wang, K. Goodson, and H. Dai, *Nano Lett.* **6**, 96 (2006).
 - [4] C. W. Chang, D. Okawa, A. Majumdar, and A. Zettl, *Science* **314**, 1121 (2006).
 - [5] N. Yang, G. Zhang, and B. Li, *Appl. Phys. Lett.* **93**, 243111 (2008).
 - [6] N. Yang, G. Zhang, and B. Li, *Appl. Phys. Lett.* **95**, 033107 (2009).
 - [7] G. Wu and B. Li, *Phys. Rev. B* **76**, 085424 (2007).
 - [8] J. Hu, X. Ruan, and Y. P. Chen, *Nano Lett.* **9**, 2730 (2009).
 - [9] D. Li, Y. Wu, P. Kim, L. Shi, P. Yang, and A. Majumdar, *Appl. Phys. Lett.* **83**, 2934 (2003).
 - [10] C. W. Chang, D. Okawa, H. Garcia, A. Majumdar, and A. Zettl, *Phys. Rev. Lett.* **101**, 075903 (2008).
 - [11] S. Maruyama, *Physica B* **323**, 193 (2002).
 - [12] G. Zhang and B. Li, *J. Chem. Phys.* **123**, 014705 (2005).
 - [13] A. V. Savin, B. Hu, and Y. S. Kivshar, *Phys. Rev. B* **80**, 195423 (2009).
 - [14] M. Endo and H. Sugiyama, *Chembiochem* **10**, 2420 (2009).
 - [15] R. K. Joshi, L. West, A. Kumar, N. Joshi, S. Alwarappan, and A. Kumar, *Nanotechnology* **21**, 185604 (2010).
 - [16] T. Kodama, A. Jain, and K. E. Goodson, *Nano Lett.* **9**, 2005 (2009).
 - [17] S. Lepri, R. Livi, and A. Politi, *Phys. Rev. Lett.* **78**, 1896 (1997).
 - [18] S. Lepri, R. Livi, and A. Politi, *Phys. Reports* **377**, 1 (2003).
 - [19] W. D. Cornell, P. Cieplak, C. I. Bayly, I. R. Gould, K. M. Merz, Jr. D. M. Ferguson, D. C. Spellmeyer, T. Fox, J. W. Caldwell, and P. A. Kollman, *J. Am. Chem. Soc.* **117**, 5179 (1995).
 - [20] N. Foloppe and A. D. MacKerell, *J. Comput. Chem.* **21**, 86 (2000).
 - [21] A. D. MacKerell and N. K. Banavali, **21**, 105 (2000).
 - [22] A. Perez, F. J. Luque, and M. Orozco, *Journal of American Chemical Society* **129**, 14739 (2007).

- [23] A. Perez, I. Marchan, D. Svozil, J. Sponer, T. E. Cheatham II, C. A. Laughton, and M. Orozco, *Biophys. J.* **92**, 3817 (2007).
- [24] A. Perez, F. Lankas, F. J. Luque, and M. Orozco, *Nucleic Acids Research* **36**, 2379 (2008).
- [25] I. Cozmuta and H. Mehrez, *J. Comp. Theor. Nanosci.* **4**, 349 (2007).
- [26] D. L. Beveridge, G. Barreiro, K. S. Byun, D. A. Case, T. E. Cheatham, S. B. Dixit, E. Giudice, F. Lankas, R. Lavery, J. H. Maddocks, et al., *Biophys. J.* **87**, 3799 (2004).
- [27] V. Makarov, B. M. Pettitt, and M. Feig, *Acc Chem Res* **35**, 376 (2002), URL <http://www.hubmed.org/display.cgi?uids=12069622>.
- [28] E. Giudice and R. Lavery, *Acc. Chem. Res.* **35**, 350 (2002).
- [29] T. E. Cheatham and P. A. Kollman, *J. Mol. Biol.* **259**, 434 (1996).
- [30] M. Feig and B. M. Pettitt, *J. Phys. Chem. B* **101**, 7361 (1997).
- [31] M. Feig and B. M. Pettitt, *Biopolymers* **48**, 199 (1998).
- [32] J. Norberg and L. Nilsson, *J. Phys. Chem.* **99**, 14876 (1995).
- [33] D. A. Case, T. E. Cheatham, T. Darden, H. Gohlke, R. Luo, K. M. Merz, A. Onufriev, C. Simmerling, B. Wang, and R. J. Woods, *J Comput Chem* **26**, 1668 (2005), URL <http://www.hubmed.org/display.cgi?uids=162006168>.
- [34] A. Pérez, J. Sponer, P. Jurecka, P. Hobza, F. J. Luque, and M. Orozco, *Chemistry* **11**, 5062 (2005), URL <http://www.hubmed.org/display.cgi?uids=15977281>.
- [35] J. Sponer, P. Jurecka, I. Marchan, F. J. Luque, M. Orozco, and P. Hobza, *Chemistry* **12**, 2854 (2006), URL <http://www.hubmed.org/display.cgi?uids=164251720>.
- [36] A. Onufriev, in *Annual Reports in Computational Chemistry*, edited by R. Wheeler and D. Spellmeyer (Elsevier, Amsterdam, The Netherlands, 2008), vol. 4, pp. 125–137.
- [37] N. A. Baker, *Curr. Opin. Struct. Biol.* **15**, 137 (2005).
- [38] C. J. Cramer and D. G. Truhlar, *Chem. Rev.* **99**, 2161 (1999).
- [39] M. K. Gilson, *Curr. Opin. Struct. Biol.* **5**, 216 (1995).
- [40] M. Scarsi, J. Apostolakis, and A. Caflisch, *J. Phys. Chem. A* **101**, 8098 (1997).
- [41] J. Z. Ruscio and A. Onufriev, *Biophys. J.* **91**, 4121 (2006).
- [42] D. F. N. Bruant, R. Lavery, and D. Genest, *Biophys. J.* **77**, 2366 (1999).
- [43] K. Drukker and G. C. Schatz, *J. Phys. Chem. B* **104**, 6108 (2000).
- [44] K. Drukker, G. Wu, and G. C. Schatz, *J. Chem. Phys.* **114**, 579 (2001).
- [45] M. Orozco, A. Pérez, A. Noy, and F. J. Luque, *Chem. Soc. Rev.* **32**, 350 (2003), URL <http://www.hubmed.org/display.cgi?uids=14671790>.
- [46] B. Mergell, M. R. Ejtehadi, and R. Everaers, *Phys. Rev. E* **68**, 021911 (2003).
- [47] S. O. Nielsen, C. F. Lopez, G. Srinivas, and M. L. Klein, *J. Phys.: Condens. Matter* **16**, R481 (2004).
- [48] Y.-L. Chen, M. D. Graham, J. J. de Pablo, K. Jo, and D. C. Schwartz, *Macromol.* **38**, 6680 (2005).
- [49] M. Sales-Pardo, R. Guimera, A. A. Moreira, J. Widom, and L. A. N. Amaral, *Phys. Rev. E* **71**, 051902 (2005).
- [50] H. L. Tepper and G. A. Voth, *J. Chem. Phys.* **122**, 124906 (2005).
- [51] C. B. Hyeon and D. Thirumalai, *Bioph. J.* **90**, 3410 (2006).
- [52] J. Errami, M. Peyrard, and N. Theodorakopoulos, *Eur. Phys. J. E* **23**, 397 (2007).
- [53] T. A. Knotts IV, N. Rathore, D. C. Schwartz, and J. J. de Pablo, *J. Chem. Physics* **126**, 084901 (2007).
- [54] M. Cadoni, R. De Leo, and G. Gaeta, *Phys. Rev. E* **75**, 021919 (2007).
- [55] N. B. Becker and R. Everaers, *Phys. Rev. E* **76**, 021923 (2007).
- [56] M. McCullagh, T. Prytkova, S. Tonzani, N. D. Winter, and G. C. Schatz, *J. Phys. Chem. B* **112**, 10388 (2008).
- [57] L. Höfler and R. E. Gyurecsat'nyi, *Electroanalysis* **20**, 301 (2008).
- [58] A. K. Mazur, *J. Phys. Chem. B* **112**, 4975 (2008).
- [59] A. K. Mazur, *J. Phys. Chem. B* **2113**, 2077 (2009).
- [60] N. A. Kovaleva, L. I. Manevitch, A. I. Musienko, and A. V. Savin, *Polymer Science* **51**, 833 (2009).
- [61] A. Morris-Andrews, J. Rottler, and S. S. Plotkin, *J. Chem. Phys.* **132**, 035105 (2010).
- [62] P. Yakovchuk, E. Protozanova, and M. D. Frank-Kamenetskii, *Nucleic Acids Res.* **34**, 564 (2006).
- [63] T. Schlick, *Molecular Modeling and Simulation* (Springer, 2002).
- [64] A. R. Leach, *Molecular Modelling: Principles and Applications*. (Addison Wesley Longman, Essex UK, 1996).
- [65] W. C. Still, A. Tempczyk, R. C. Hawley, and T. Hendrickson, *J. Am. Chem. Soc.* **112**, 6127 (1990).
- [66] V. Tsui and D. Case, *J. Am. Chem. Soc.* **122**, 2489 (2000).
- [67] D. Bashford and D. A. Case, *Annu. Rev. Phys. Chem.* **51**, 129 (2000).
- [68] J. Chocholousova and M. Feig, *J. Phys. Chem. B* **110**, 17240 (2006).
- [69] C. Keslo and C. Simmerling, in *Computational Studies of RNA and DNA*, edited by J. Sponer and F. Lankas (Springer, Dordrecht, The Netherlands, 2006), vol. 2 of *Challenges and Advances in Computational Chemistry and Physics*, pp. 147–167.
- [70] M. Zacharias, in *Computational Studies of RNA and DNA*, edited by J. Sponer and F. Lankas (Springer, Dordrecht, The Netherlands, 2006), vol. 2 of *Challenges and Advances in Computational Chemistry and Physics*, pp. 95–119.
- [71] L. Wang, B. E. Hingerty, A. R. Srinivasan, W. K. Olson, and S. Broyde, *Biophys J* **83**, 382 (2002), URL <http://www.hubmed.org/display.cgi?uids=12080128>.
- [72] V. Tsui and D. Case, *Biopolymers* **56**, 275 (2001).
- [73] E. Sorin, Y. Rhee, B. Nakatani, and V. Pande, *Biophys J* **85**, 790 (2003), URL <http://www.hubmed.org/display.cgi?uids=12885628>.
- [74] A. Balaeff, M. E. Churchill, and K. Schulten, *Proteins* **30**, 113 (1998), URL <http://www.hubmed.org/display.cgi?uids=9489920>.
- [75] B. Jayaram, K. McConnell, S. B. Dixit, A. Das, and D. L. Beveridge, *J Comput Chem* **23**, 1 (2002), URL <http://www.hubmed.org/display.cgi?uids=11913374>.
- [76] L. F. De Castro and M. Zacharias, *J Mol Recognit* **15**, 209 (2002), URL <http://www.hubmed.org/display.cgi?uids=12382239>.
- [77] H. Allawi, M. Kaiser, A. Onufriev, W. Ma, A. Brogaard, D. Case, B. Neri, and V. Lyamichev, *J. Mol. Biol.* **328**, 537 (2003).
- [78] A. Onufriev, D. A. Case, and D. Bashford, *Journal of Computational Chemistry* **23**, 1297 (2002).
- [79] J. Srinivasan, M. Trevathan, P. Beroza, and D. Case, *Theor. Chem. Accts* **101**, 426 (1999).
- [80] B. K. P. Horn, *J. Opt. Soc. Am. A* **4**, 629 (1987).
- [81] H. R. Drew, R. M. Wing, T. Takano, C. Broka, S. Tanaka, K. Itakura, and R. E. Dickerson, *Proc. Natl. Acad. Sci. USA* **78**, 2179 (1981).
- [82] X.-J. Lu and W. K. Olson, *Nucleic Acids. Res.* **31**, 5108 (2003).
- [83] R. Dickerson, *Nucleic acids in International Tables for Crystallography* (Kluwer Academic Publishers, 2001), vol. F of *Crystallography of Biological Macromolecules*, pp. 588–622.
- [84] P. Cluzel, A. Lebrun, A. Heller, R. Lavery, J.-L. Viovy, D. Chatenay, and F. Caron, *Science* **271**, 792 (1996).

- [85] S. B. Smith, Y. Cui, and C. Bustamante, *Science* **271**, 795 (1996).
- [86] C. Bustamante, S. B. Smith, J. Liphardt, and D. Smith, *Current Opinion in Structural Biology* **10**, 279 (2000).
- [87] H. Clausen-Schaumann, M. Rief, C. Tolksdorf, and H. E. Gaub, *Biophys. Journal* **78**, 1997 (2000).
- [88] A. Lebrun and R. Lavery, *Nucleic Acids Research* **24**, 2260 (1996).
- [89] Z. Bryant, M. D. Stone, J. Gore, and S. B. Smith, *Nature* **424**, 338 (2003).
- [90] M. B. Hakim, S. M. Lindsay, and J. Powell, *Biopolymers* **23**, 1185 (1984).
- [91] M. Krisch, A. Mermet, H. Grimm, V. T. Forsyth, and A. Rupprecht, *Phys. Rev. E* **73**, 061909 (2006).
- [92] S. Buyukdagli, A. V. Savin, and B. Hu, *Phys. Rev. E* **78**, 066702 (2008).
- [93] H. Dammak, Y. Chalopin, M. Laroche, M. Hayoun, and J.-J. Greffet, *Phys. Rev. Lett.* **103**, 190601 (2009).
- [94] O. V. Gendelman and A. V. Savin, *Phys. Rev. Lett.* **84**, 2381 (2000).
- [95] C. Giardina, R. Livi, A. Politi, and M. Vassalli, *Phys. Rev. Lett.* **84**, 2144 (2000).